Steepness-fragility insights from the temperature derivative analysis of dielectric data of a highly nonsymmetric liquid crystal dimer

Josep Salud [1], Nerea Sebastián [2], María R. de la Fuente [3], S. Diez-Berart [1], and David O. López [1,*]

[1] *Grup de Propietas Físiques dels Materials (GRPFM), Departament de Física, E.T.S.E.I.B. Universitat Politècnica de Catalunya. Diagonal 647, E- 08028 Barcelona, Spain*

[2] *Jožef Stefan Institute, Jamova cesta 39, SI-1000 Ljubljana, Slovenia*

[3] *Departamento de Física Aplicada II, Facultad de Ciencia y Tecnología, Universidad del País Vasco, Apartado 644, E-48080 Bilbao, Spain*

(Received 30 April 2024; accepted 18 July 2024; published 12 August 2024)

A comprehensive dynamic analysis of the dielectric relaxation-time data across a broad temperature range for both isotropic and nematic phases has been conducted on the *CBO3O.Py* liquid crystal dimer, the shorter chain-length compound within the highly nonsymmetric pyrene-based series of liquid crystal dimers (*CBOnO.Py*, with *n* ranging from 3 to 11). It was known from another previous study that in the nematic phase, three different relaxation processes contribute to the complex dielectric permittivity depending on the orientation of the alignment axis with respect to the probing electric field direction. The temperature-derivative analysis of the relaxation-time data using different analytic functions reveals that the critical-like description, through the dynamic scaling model, best portrays the relaxation-time data in the nematic phase as the system approaches the glass transition. A single glass transition temperature is obtained which is consistent with thermal stimulated depolarization currents experimental determinations published elsewhere. From temperature-dependent steepness index *m(T)*, the activation-critical model is also considered as a more general analytic function from which the dynamic scaling model is a terminal approximation. Additionally, the critical-like parametrization provides insight into obtaining a universal description of the temperature-dependent steepness index *m(T),* for all liquid crystal compounds belonging to symmetry-selected glass formers, such as rodlike liquid crystal monomers.

DOI: 10.1103/PhysRevE.110.024702

I. INTRODUCTION

The liquid crystal materials list has substantially increased in the last decades due to the constant chemical work in proposing new molecular architectures and in turn, new mesophases with potential technological applications have been observed. From such a list, a group of materials usually denoted as liquid crystal dimers has deserved our attention in the last decade because of their rich variety of molecular motions consequence of their molecular flexible geometry. In some of these materials, one of the mesophases can exhibit the ability to be supercooled in a way that the molecular motions are forced to freeze, becoming a glassy state, a fact which takes place at the glass transition temperature (T_g). The molecular dynamics and the possibility to freeze the dynamic disorder at low enough temperatures have been thoroughly studied in several ways either by modulated differential scanning calorimetry, broadband dielectric spectroscopy (BDS), or thermal stimulated depolarization currents (TSDC) [1–10].

Liquid crystal dimers are a type of liquid crystals in which the molecular architecture is formed by two semirigid units, either different or identical, linked by a flexible spacer, mostly alkyl chains [11]. This molecular structure provides them with several degrees of flexibility due to the length and parity of the spacer giving the possibility to adopt different molecular conformations with temperature. As a consequence, they have shown a renewed interest because of some new findings. Among others, it is known that molecular curvature and flexibility are factors that seem to play a crucial role in the existence of a new mesophase denoted as twist-bend nematics, first identified experimentally in the 1″, 7″-bis (4-cyanobiphenyl-4′-yl) heptane (also denoted as *CB7CB*) liquid crystal dimer [12]. Liquid crystal dimers have also allowed to observe blue phases over a wide temperature range [13] and several glass transition temperatures associated with different molecular motions in the same compound [4,9,10].

Among the list of liquid crystal dimers, the series of highly nonsymmetric pyrene-based compounds α-(4-cyanobiphenyl-4′-oxy)-ω-(1-pyreniminebenzylidene-4′- oxy) alkanes (*CBOnO.Py*), with odd *n* ranging from 3 to 11, have revealed a complex molecular dynamics but a richer variety of molecular motions in every compound. Several decades ago, Attard and co-workers showed interest in *CBOnO.Py* as glass formers in a preliminary study concerning their chemical synthesis and mesophase behavior [14]. Nearly 20 years later, an extensive experimental study was conducted using BDS [2–4,10] and to a lesser extent, TSDC [9] and deuteron nuclear magnetic resonance [15]. From these measurements, a successful interpretation of the different molecular motions

*Contact author: david.orencio.lopez@upc.edu

 ©2024 American Physical Society

was possible with the aid of the theoretical approach proposed by Stocchero *et al.* [16], as well as with the old theoretical findings published for monomeric liquid crystals [17,18]. While all odd *CBOnO.Py* compounds exhibit glass transition, only two of them ($n = 3$ and 7) can be slowly supercooled from a mesophase, reaching the glassy state without any crystallization. This fact is of great importance because it is possible to observe how the characteristic dielectric relaxation time $\tau(T)$ of the identified motions changes over a wide range of temperatures. Thus, the temperature dependence of dynamic models can be successfully tested throughout the entire temperature range down to the glass transition.

Regarding the *CBO7O.Py* liquid crystal dimer, a study was published a few years ago in which the derivative analysis of the dielectric relaxation time $\tau(T)$ for the identified motions allowed the detection of dynamic crossovers [10]. As a striking result, two glass transitions associated with the three identified molecular motions have been confirmed.

In the present study, our focus has been on the *CBO3O.P*y liquid crystal dimer. Previously, in the analyzed range, the temperature dependence of the characteristic relaxation frequencies (or relaxation times) of the dielectric permittivity associated with the different molecular motions was clearly observed as non-Arrhenius, in contrast to the other odd *CBOnO.Py* compounds with a longer spacer [3]. In fact, *CBO3O.P*y shares similarities with ordinary rodlike nematic liquid crystals, and the non-Arrhenius behavior of relaxation times in such compounds is usually described by the empirical Vogel-Fulcher-Tammann (VFT) relationship [19–21]:

$$\tau(T) = \tau_0^{\mathrm{VFT}} \exp\left[\frac{B}{T - T_0}\right], \tag{1}$$

where τ_0^{VFT} is the relaxation time in the high-temperature limit, B is an activation parameter expressed in kelvin, and T_0 is the ideal glass transition temperature, also called Vogel temperature. The formalism of the VFT equation can also be inferred in glass-forming liquids, either from the free-volume approach [22] or from the Adam-Gibbs molecular-kinetic theory based on the concept of molecular clusters or regions that must collectively rearrange as the glass transition approaches. These are commonly referred to as cooperatively rearranged regions [23]. It should be stressed that the VFT law implies a divergence of the relaxation time at T_0, and its applicability to glass formers is controversial [24–27]. It has also been shown that it is not the best choice in portraying relaxation times of other closely related liquid crystalline glassy systems [1,10].

It seems accepted as a general feature of glass formers that their dynamics on cooling close to the glass transition is governed by spatially correlated cooperative rearranging regions. The length scale (ξ) of such spatially heterogeneous dynamics depends on temperature, and Souletie [28] and Colby [29,30] suggested a power-law dependence $[(T - T_C)/T_C]^{-\nu}$ based on a "critical point" at T_C located below the glass transition temperature where the size of the heterogeneous regions diverges. Thus, the temperature evolution of dynamic properties, i.e., relaxation times (or viscosity for liquids), is given, according to the "absolute definition," by the relationship [28–30]

$$\begin{aligned}\tau(T) &= \tau_0^{\mathrm{DS}} \left(\frac{\xi(\mathrm{T})}{\xi_0}\right)^{-z} \\ &= \tau_0^{\mathrm{DS}} \left(\frac{T - T_C}{T_C}\right)^{-\nu z} \\ &= \tau_0^{\mathrm{DS}} \left(\frac{T - T_C}{T_C}\right)^{-\phi},\end{aligned} \tag{2a}$$

or according to the "relative definition" [31–33]:

$$\tau(T) = \tau_0^{\mathrm{DS}} \left(\frac{T - T_C}{T}\right)^{-\phi}, \tag{2b}$$

where $T < T_A$, DS is dynamic scaling, τ_0^{DS} is the relaxation time at $2T_C$, and T_A is the caging temperature, a temperature considered as the limit above which the cooperative rearranging motions become less important and disappear. According to the DS model [29,30], the exponents ν and z are set equal to 3/2 and 6, respectively. Thus, the power exponent ϕ has the DS model universal value of 9 for all glass-forming liquids and polymers [34]. However, experimental results on a great variety of glass formers give values of ϕ that sometimes strongly differ from 9. Drozd-Rzoska *et al.* [34] claim for the validity of Eq. (2a) with the exponent $\phi = 9$ for symmetry-selected glass formers, and rodlike nematic liquid crystals are one of the molecular-type model materials that meet this requirement. The application of Eq. (2a) for the vitrification of other liquid crystal dimers has been tested, obtaining values of ϕ ranging from 6 to 8 [1,10]. This approach has shown some additional advantages over the VFT description, including the matching of glass transition temperatures with those observed by means of the TSDC technique [4,9]. Regrettably, such studies are scarce due to the limited number of liquid crystal dimers that vitrify at relatively slow cooling rates.

The high-temperature dynamic domain at temperatures above T_A could also be well parametrized by a critical-like relationship similar to that of Eq. (2) but in the framework of the mode-coupling theory (MCT) [35,36], namely:

$$\tau(T) = \tau_0^{\mathrm{MCT}} \left(\frac{T - T_C^{\mathrm{MCT}}}{T_C^{\mathrm{MCT}}}\right)^{-\phi'}, \quad T > T_C^{\mathrm{MCT}} + 20, \tag{3}$$

where τ_0^{MCT} is the relaxation time at $2T_C^{\mathrm{MCT}}$. The temperature T_C^{MCT} is related to the crossover temperature from the ergodic to the nonergodic domain, which may be correlated with T_A. The power exponent ϕ' ranges from 1.4 to 4 [34,37]. Recently, it has been claimed that the MCT description is a powerful tool to account for the experimental dynamic behavior in rodlike nematic liquid crystals because they are considered as an experimental fluid model system of hard ellipsoids of revolution [34,38].

Another topic when discussing the dynamics in glass formers is the *fragility* concept, introduced to classify the way a material becomes glass or glassy through universal dynamic features [39–41]. It has been stressed that the same material can exhibit several glass transitions associated with different dynamically disordered phases [42,43], and even for a given disordered phase, several glass transitions can be identified

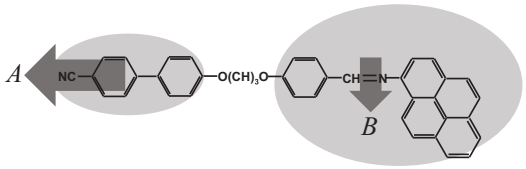

FIG. 1. Scheme of the molecular structure of *CBO3O.Py* liquid crystal dimer. The arrows A and B represent the dipole moment vector associated with the nitrile group and the dipole moment vector associated with the imine group, respectively.

with different molecular motions [10]. Thus, the fragility concept should be applied to the motion of a disordered phase that is frozen at the glass transition, and this increases the complexity in its quantification. One of the most extended metrics to quantify fragility is the m fragility or steepness index [44,45], defined as

$$m = \left.\frac{d\,\log_{10}\tau(T)}{d\left(\frac{T_g}{T}\right)}\right]_{T=T_g}. \tag{4}$$

Equation (4) provides information about the fragility at the glass transition temperature. However, it is sometimes convenient to introduce the temperature-dependent steepness index $m(T)$ [46] as

$$m(T) = \frac{d\,\ln\tau(T)}{d(T^{-1})}\frac{\log_{10}e}{T_g}. \tag{5}$$

Equation (5) becomes Eq. (4) after substitution of T by T_g and has the advantage of providing information on dynamic features not only just at the glass transition but also as the glassy state approaches.

The structure of the paper is as follows. In Sec. II we describe the material characteristics, experimental details, and the data analysis procedure. In Sec. III, the results concerning the temperature-derivative analysis of the relaxation-time data are presented and discussed. One part of the discussion is devoted to a universal description of the temperature-dependent steepness index $m(T)$ for symmetry-selected glass formers. Finally, a summary of the most important concluding remarks is presented.

II. EXPERIMENTAL DETAILS AND DATA ANALYSIS

A. Experimental details

The molecular structure of *CBO3O.P*y liquid crystal dimer is schematized in Fig. 1. It comprises a flexible alkyl chain consisting of three methylene units that connect two terminal groups of different shapes and sizes. As it can be observed from Fig. 1, one dipole moment vector along the long molecular axis is associated with the nitrile group, while another smaller dipole moment is observed along the short molecular axis, linked to the imine group. The material was synthesized following the methodology outlined in the work of Attard *et al.* [14].

The thermal behavior of *CBO3O.P*y liquid crystal dimer [3] was reported earlier. When the sample is heated from the crystal state (Cr), it transforms directly to the isotropic state (I) at 465.4 K without exhibiting mesogenic behavior [3]. However, when cooled from the I state, the sample undergoes the I-N phase transition at 388 K, and the N phase persists down to the glass transition, even at very slow cooling rates or under isothermal steps, as a stable phase [3]. Upon subsequent heating, the N phase is maintained until the N-I phase transition occurs at 388 K. It should be stressed that if the sample is heated up after the N-I phase transition, the I state irreversibly crystallizes at about 415 K [3].

The complex dielectric permittivity measurements were conducted over a broad frequency range 10^{-2}–1.9×10^{9} Hz Hz using two complementary impedance analyzers: an HP4291A (frequency range 10^{6}–1.9×10^{9} Hz) and an Alpha from Novocontrol (frequency range 10^{-2}–10^{6} Hz). The measurement cell consisted of two gold-plated brass electrodes of diameter 5 mm separated by 50-μm-thick silica spacers in a cryostat from Novocontrol. The cryostat allowed for computer-controlled temperature and frequency adjustments. The experiments involved cooling the sample with stabilization at different temperature steps, with a temperature-control precision of about 20 mK. Further details of the technique can be found elsewhere [3,43,47].

B. Data analysis

The main objective is to determine the most suitable formulation to describe the experimental dynamic data, specifically the dielectric relaxation time with temperature, in the *CBO3O.P*y liquid crystal dimer. In this study, both the VFT equation [Eq. (1)] and the critical-like parametrization equations (2) and (3) are considered. The methodology proposed by Stickel *et al.* [48,49], which involves the temperature-derivative analysis of the relaxation-time data, is employed for this purpose.

The temperature-derivative analysis applied to Eq. (1) [46] leads to

$$\left[\frac{d\,\ln\tau(T)}{d(1/T)}\right]^{-(1/2)} = \left[\frac{H_A(T)}{R}\right]^{-(1/2)} = B^{-(1/2)}\left(1-\frac{T_0}{T}\right), \tag{6}$$

where R is the gas constant, and $H_A(T)$ is the apparent activation enthalpy [38,46]. The validity of Eq. (1) to portray the experimental $\tau(T)$ data is displayed by a linear dependence of the $[H_A(T)]^{-(1/2)}$ on inverse temperature.

Similarly, the temperature-derivative analysis applied to the critical-like description through Eqs. (2a) and (3) [46] leads to

$$T^2\left[\frac{d\,\ln\tau}{d(1/T)}\right]^{-1} = \left[\frac{T^2R}{H_A(T)}\right] = \frac{1}{\Theta}\left(T-T_C^X\right), \tag{7}$$

where T_C^X accounts for either T_C^{DS} in the dynamic scaling model (DSM) parametrization [Eq. (2)] or T_C^{MCT} in the MCT description [Eq. (3)], and Θ is either ϕ (DSM equation) or ϕ' (MCT equation). The validity of the critical-like description [in the domain where both Eqs. (2) and (3) are applicable] to describe the experimental $\tau(T)$ data requires a linear dependence of $[T^2/H_A(T)]$ on temperature.

III. RESULTS AND DISCUSSION

A. Dielectric relaxation times

In the present paper, additional dielectric data for *CBO3O.Py* have been obtained to supplement the previously published partial data [3]. These data cover both the high-temperature range in the isotropic state (*I* state) and the low-temperature range, close to the glass transition.

In the previous work on *CBO3O.Py* [3], dielectric spectra with the sample in metallic cells were obtained in parallel alignment ($\parallel$), meaning that the director is aligned parallel to the probing electric field, by the application of a dc bias voltage of 35 V over the complete temperature range. In the absence of dc bias voltage, the perpendicular component of the permittivity ($\perp$) was obtained. The experimental complex permittivity $[\varepsilon(\omega)]$ has been fitted to the empirical relationship:

$$\varepsilon(\omega) = \sum_k \frac{\Delta\varepsilon_k}{[1 + (i\omega\tau_{k,\mathrm{HN}})^{\alpha_k}]^{\beta_k}} + \varepsilon_\infty - i\frac{\sigma_{\mathrm{dc}}}{\omega\varepsilon_0}, \qquad (8)$$

where the summation is extended over the identified relaxation modes and each one is fitted to the so-called Havriliak-Negami (HN) function. The fitted parameters are $\Delta\varepsilon_k$, which is the dielectric strength of each relaxation mode; $\tau_{k,\mathrm{HN}}$, which is the HN relaxation time related to the frequency of maximum dielectric loss; σ_{dc}, which is the dc conductivity; and α_k and β_k parameters that account for the shape (symmetry and width) of the relaxation spectra.

In the *I* phase, the dielectric relaxation spectra show two relaxation processes identified with the individual flip-flop reorientations of the terminal rigid units of the dimer. This is a consequence of an asymmetry between *trans*-and-*cis* conformer populations [3]. The lower relaxation is identified with the bulkier rigid unit (see Fig. 1) flip-flop reorientations (hereafter denoted as $\mu_{1,\mathrm{L}}$) and the other relaxation identified with the less bulky unit (see Fig. 1) flip-flop reorientations (hereafter referred to as $\mu_{1,\mathrm{H}}$). For $\mu_{1,\mathrm{L}}$ relaxation mode, α and β parameters according to Eq. (8) are set equal to 1 (Debye-like behavior) over the complete temperature range of analysis. For $\mu_{1,\mathrm{H}}$ relaxation mode, the α parameter according to Eq. (8) is found to be 0.8 and the β parameter ranges from 0.85 to 0.7, over the complete temperature range of analysis.

In the *N* phase, the parallel component of the permittivity was interpreted according to three relaxation processes. The two at lower frequencies were identified with the individual flip-flop reorientations of the terminal rigid units ($\mu_{1,\mathrm{L}\parallel}$ and $\mu_{1,\mathrm{H}\parallel}$), while the other at higher frequencies was mainly related to the rotation of the molecule along its molecular long axis ($\mu_{2\parallel}$) [3]. The first two relaxations ($\mu_{1,\mathrm{L}\parallel}$ and $\mu_{1,\mathrm{H}\parallel}$) predominate over the other ($\mu_{2\parallel}$) at any temperature, and even at sufficiently low temperatures (see top-left inset of Fig. 2 as an example), the $\mu_{2\parallel}$ mode is impossible to observe due to its very low amplitude. Thus, this relaxation mode will not be taken into account in our study. Solid lines in the top-left inset of Fig. 2 are fittings according to Eq. (8). The fitting parameters α and β, according to Eq. (8), for the $\mu_{1,\mathrm{L}\parallel}$ and $\mu_{1,\mathrm{H}\parallel}$ relaxation modes are set equal to 1 (Debye-like behavior) over the complete temperature range.

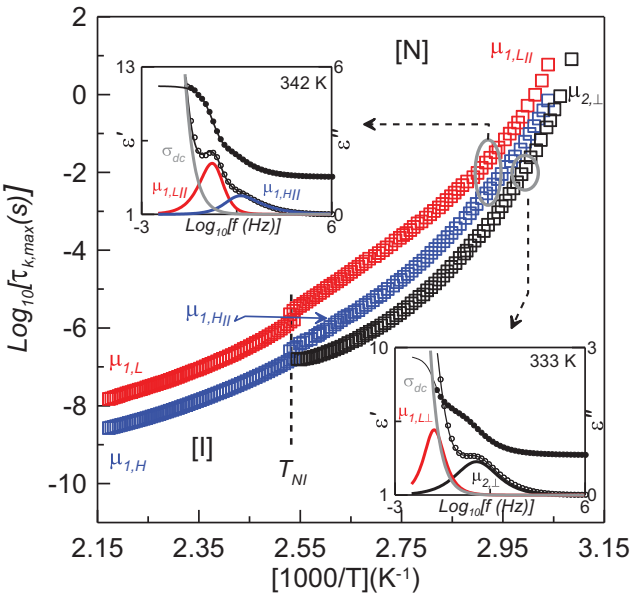

FIG. 2. Relaxation times at the frequency of maximum dielectric loss for the different relaxation modes $\mu_{1,\mathrm{L}\parallel}$, $\mu_{1,\mathrm{H}\parallel}$, and $\mu_{2\perp}$ as a function of temperature. The insets show, as examples in the nematic mesophase, the frequency dependence of the complex dielectric permittivity of *CBO3O.Py* at 342 K (top inset) and 333 K (bottom inset) for homeotropic and planar alignments, respectively. In the insets, full and empty circles account for experimental real and imaginary parts of the dielectric permittivity, respectively; black lines are fits to Eq. (8), and thick lines correspond to the contributing modes: red for $\mu_{1,\mathrm{L}\parallel}$, blue for $\mu_{1,\mathrm{H}\parallel}$, and black for $\mu_{2\perp}$.

In the *N* phase, the perpendicular component of the permittivity (see bottom-right inset of Fig. 2 as an example) was interpreted according to a main relaxation process associated with the rotation of the molecule along its molecular long axis ($\mu_{2\perp}$). However, due to a certain degree of misalignment of the sample, a residual relaxation identified with the $\mu_{1,\mathrm{L}}$ mode remains [3]. When decreasing in temperature, the $\mu_{1,\mathrm{L}}$ mode is difficult to fit due to overlap with dc conductivity, and it will not be taken into account in our study. Solid lines in the bottom-right inset of Fig. 2 are fittings according to Eq. (8). The fitting α parameter according to Eq. (8) for the $\mu_{2\perp}$ relaxation mode ranges from 0.7 to 1 and the β parameter ranges from 0.76 to 0.5, over the complete temperature range of analysis.

Figure 2 shows the relaxation time ($\tau_{k,\mathrm{max}}$) at the frequency of the maximum dielectric loss of each chosen representative relaxation mode ($\mu_{1,\mathrm{L}\parallel}$ and $\mu_{1,\mathrm{H}\parallel}$ and $\mu_{2\perp}$ for $k = 1$, 2, and 3, respectively) in an Arrhenius plot.

It should be stressed that $\tau_{k,\mathrm{max}}$ have been obtained through the formula [46]

$$\tau_{k,\mathrm{max}} = \tau_{k,\mathrm{HN}}\left[\sin\frac{\pi\alpha_k}{2+2\beta_k}\right]^{-(1/\alpha_k)}\left[\sin\frac{\pi\alpha_k\beta_k}{2+2\beta_k}\right]^{-(1/\alpha_k)}, \qquad (9)$$

where $\tau_{k,\mathrm{HN}}$, α_k, and β_k have the meanings cited above and they have been obtained from the fitting of the experimental

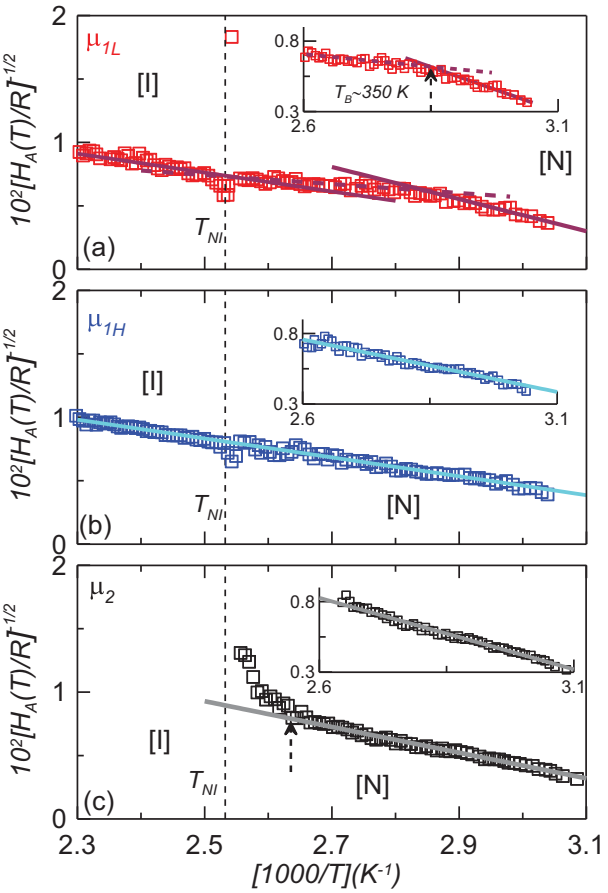

FIG. 3. Results of the temperature-derivative analysis according to Eq. (6) applied to $\mu_{1,L}$ (a), $\mu_{1,H}$ (b), and μ_2 (c) modes of *CBO3O.Py*. The insets show a zoom view to observe possible crossover behaviors and several dynamic regimes. The dashed vertical arrow in the inset of (a) for the $\mu_{1,L}$ mode indicates the separation between two dynamic domains.

complex dielectric spectra to Eq. (8). It can be observed that in the *N* phase at lower temperatures, the relaxation time of the different modes tends to merge, but it is not clear if all modes really freeze at the same glass transition temperature. It is worth recalling that TSDC studies identify only one T_g for the different molecular motions [9].

B. Volger-Fulcher-Tammann description

The VFT parametrization of the results via the temperature-derivative analysis through Eq. (6) is shown in Fig. 3 for each selected dielectric mode, $\mu_{1,L}$ and $\mu_{1,H}$ both obtained in parallel alignment, and μ_2 obtained from perpendicular alignment. As mentioned earlier, on the plot of $[H_A(T)]^{-(1/2)}$ vs inverse temperature, the VFT behavior is satisfied by a sloping straight line in which the slope is related to $B^-(1/2)T_0$ of Eq. (1). Of course, if the Vogel temperature T_0 is zero (Arrhenius behavior), a nonsloping line would be expected.

Regarding the $\mu_{1,L}$ mode [see Fig. 3(a)], in the *N* phase, a sloping change in the straight line at about 350 K (2.86 in 1000/*T*) suggests two dynamic domains, with the crossover temperature (T_B) being this sloping change. Table I lists both *B* and T_0 fitted parameters of both VFT dynamic domains after a refinement procedure using Eq. (1) to obtain the prefactor τ_0^{VFT}. This crossover seems to be nonexistent for the other two modes ($\mu_{1,H}$ and μ_2) as observed in the insets of Figs. 3(b) and 3(c).

Both *B* and T_0 fitted parameters, after a refinement procedure using Eq. (1) to obtain the prefactor τ_0^{VFT}, are very close to those obtained for the *N* phase and are listed in Table I. The VFT dynamic domain corresponding to the *I* phase of the $\mu_{1,L}$ mode is described by the same parameters as those obtained for the $\mu_{1,H}$ mode, and thus, the refined *B* and T_0, including the prefactor τ_0^{VFT} through Eq. (1), are very close to those corresponding to the $\mu_{1,H}$ mode (see Table I).

The μ_2 mode is only observed in the *N* phase and out of the transition region [its lower limit has been pointed out by the arrow in Fig. 3(c)], exhibits a single VFT dynamic domain. The corresponding *B* and T_0 parameters refined by using Eq. (1) together with the prefactor τ_0^{VFT} are listed in Table I.

Figure 4 shows the relaxation-time data plotted against the inverse of temperature, accompanied by VFT fittings of the different dynamic domains according to the parameters listed in Table I. The glass transition temperature, according to the VFT parametrization, varies slightly for each relaxation mode within a 3 K range, ranging from 320.7 K for the $\mu_{1,H}$ mode to 323.7 K for the $\mu_{1,L}$ mode. In this last case, it is interesting to note the low value of the order of 10^{-7} s for the prefactor τ_0^{VFT}. An interesting observation from the inset of Fig. 4 is that the apparent activation enthalpies associated with the different modes tend to converge between 385 and 374 K, remaining nearly indistinguishable from this temperature down to the glass transition.

C. Critical-like parametrization

The critical-like description, applied to τ data through temperature-derivative analysis using Eq. (7), is shown in Fig. 5 for each selected dielectric mode. This includes $\mu_{1,L}$ and $\mu_{1,H}$, both acquired in parallel alignment, as well as μ_2 obtained from perpendicular alignment. As discussed earlier, the validation of that description requires a linear trend on the plot of $[T^2R/H_A(T)]$ against temperature. Figure 5 unequivocally exhibits a linear trend for both $\mu_{1,L}$ and $\mu_{1,H}$ modes throughout the *N* mesophase, spanning from glass transition (T_g) up to the *N-I* phase transition, and even in the *I* phase. However, the μ_2 mode in all the *N*-mesophase range shows two distinct linear trends. One extends from T_g up to about 373 K, while the other is at higher temperatures, identifying 373 K as the so-called caging temperature T_A. It is evident how the low-temperature linear trend for the μ_2 mode matches up with that of the other $\mu_{1,L}$ and $\mu_{1,H}$ modes. Preliminary linear fittings based on Eq. (7) for each mode yield values of Θ around 9, a value compatible with the DSM parametrization for symmetry-selected glass formers. A tentative linear fitting to the high-temperature part of the μ_2 mode (373 K to near the *N-I* phase transition, excluding points very close to the transition) provides a Θ-value of 1.5, compatible with the MCT description. The refined fitting parameters, considering Eqs. (2a) and (3) with the prefactor τ_0^X (where *X* represents

TABLE I. Fitting parameters according to Eq. (1) for the different dynamic domains and the calculated glass transition temperature for the $\mu_{1,L}$, μ_{1H}, and μ_2 modes of *CBO3O.Py* liquid crystal dimer.

Phase	Mode	$\log10[\tau_0^{VFT}(s)]$	B (K)	T_0 (K)	T_g (K)	Range $[1000/T\,(K^{-1})]$	χ^2
Isotropic	$\mu_{1,L}$	−11.15	1402.8	278.6		2.17–2.52	0.001
	$\mu_{1,H}$	−11.70	1333.7	275.2		2.17–2.52	0.0002
Nematic	$\mu_{1,L}$[a]	−14.82	3767.7	217.6		2.53–2.86	0.0001
		−6.94	549.7	297.0	323.7	2.86–3.04	0.007
	$\mu_{1,H}$	−11.58	1379.8	276.6	320.7	2.55–3.04	0.0006
	μ_2	−10.64	833.4	292.8	321.4	2.65–3.08	0.002

[a]Dynamic crossover at about $T_B \approx 350$ K.

either DS or MCT), are listed in Table II. The inset of Fig. 5, depicted in an Arrhenius plot, shows how the experimental data are well portrayed by the fitting curves constructed with the parameters outlined in Table II.

Observing Table II, it is evident that the critical-like description yields comparable values for the glass transition in the three relaxation modes, with a temperature difference of less than 1 K. This result aligns with the reporting of only one glass transition temperature for the three relaxation modes by TSDC [9], as previously mentioned.

On the other hand, as stressed for *CBO7O.P*y [10], a compound with a longer chain length in the same series, and also for the symmetric dimer *CB7CB* [1], motions identified with μ_1 relaxation modes (either $\mu_{1,L}$ or $\mu_{1,H}$) are highly cooperative. This cooperativity is not limited to the vicinity of the glass transition but extends throughout the entire temperature range of the *N* mesophase. As already cited elsewhere [1,10], the anisotropic environment favors intermolecular cooperativity for flip-flop motions of terminal rigid units at any temperature. However, μ_2 relaxation modes, identified with the rotation of the molecule along its molecular long axis, show the loss of intermolecular cooperativity in the *N* mesophase at T_A, the caging temperature. This temperature is approximately $1.03T_C^{MCT}$ or $1.2T_C^{DS}$ (≈373 K), closely resembling the temperature range reported by Erwin and Colby [30]. This behavior aligns with observations in nonsymmetric dimer *CBO7O.P*y and symmetric dimer *CB7CB* [1,10].

There still remains a fact to stress from Fig. 5. Both $\mu_{1,L}$ and $\mu_{1,H}$ data from the *I* phase show linear trends compatible with the MCT model, with an extrapolated T_C^{MCT} of about 360 K. Interestingly, this value is virtually the same as T_C^{MCT} for μ_2 data, as observed in Table II. It is worth noting that $T_C^{MCT} \approx T_{NI} - 30$ K, a pattern observed in other rodlike nematic liquid crystals [34].

D. Temperature-dependent steepness index

Fragility, as indicated by the temperature-dependent steepness index *m(T)* in Eq. (5), serves as an excellent test for understanding the dynamic features of *CBO3O.P*y as it approaches the glassy state. Figure 6 shows *m (T)* against temperature for each selected dielectric mode, $\mu_{1,L}$, $\mu_{1,H}$, and μ_2. Looking closely at Fig. 6, only one fragility for the *N*

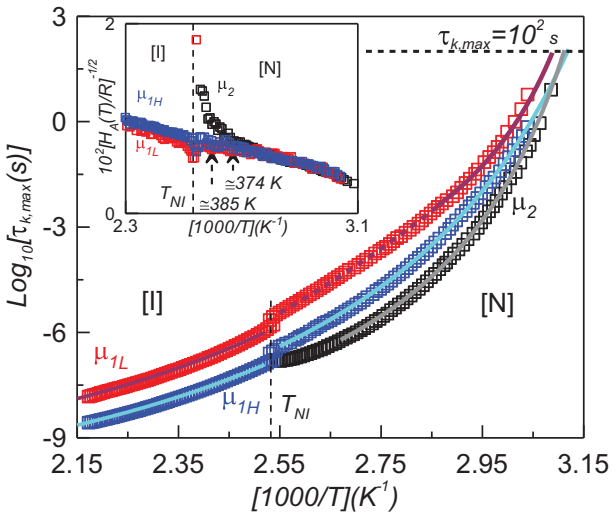

FIG. 4. Relaxation-time data for the different modes as an Arrhenius plot. Colored lines are drawn according to Eq. (1) with the parameters listed in Table I. The inset shows the same information as Fig. 3, but with the three relaxation modes in the same plot.

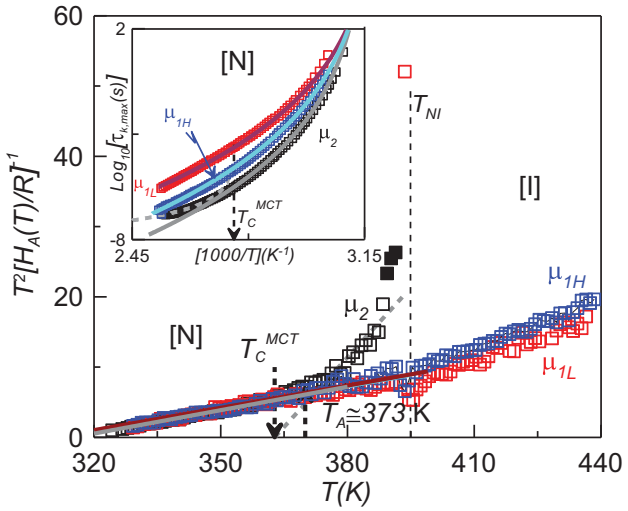

FIG. 5. Results of the temperature-derivative analysis according to Eq. (7) applied to $\mu_{1,L}$, $\mu_{1,H}$, and $\mu_{2\perp}$ modes of *CBO3O.Py*. The inset shows the relaxation-time data of the different modes as an Arrhenius plot. Solid and dashed lines correspond to the dynamic domains for the different modes calculated using Eqs. (2a), (3), and (7) with the parameters listed in Table II.

TABLE II. Fitting parameters according to Eqs. (2a) and (3) for the different dynamic domains and the calculated glass transition temperature for the $\mu_{1,L}$, μ_{1H}, and μ_2 modes of *CBO3O.Py* liquid crystal dimer.

Mode	$\log_{10}[t_0(s)]$	T_C^X (K)	ϕ	T_g (K)	Range [1000/T (K^{-1})]	Description	χ^2
$\mu_{1,L}$	−10.52	311 ± 4	8.9 ± 0.3	322.9	2.53–3.04	DS	0.001
$\mu_{1,H}$	−11.98	313 ± 2	9.3 ± 0.3	322.4	2.53–3.04	DS	0.001
μ_2	−8.46	362.7	1.5		2.53–2.67	MCT	0.0002
	−12.90	315 ± 1	9.0 ± 0.3	322.2	2.67–3.09	DS	0.001

mesophase seems to be suggested, regardless of the considered molecular motion. If we set $T = T_g$ in Eq. (5) and refer to Fig. 6, the m fragility according to Plazek *et al.* [44,45] is retrieved with a value around 165. This value, however, comes with a certain degree of uncertainty due to the asymptotic behavior observed at T_g. In Ref. [3], a tentative and underestimated m value of about 100 was published, considering only partial τ dielectric data for both $\mu_{1,L}$ and $\mu_{1,H}$ dielectric modes, which were evidently too far from the glass transition temperature.

The inset of Fig. 6 shows $[m(T)]^{-1}$ against the inverse of temperature. A common linear trend is evident from the glass transition temperature to the cage temperature (T_A), regardless of the mode. This fact is fully compatible with the DS model, as explained in the following. Combining Eq. (5) with Eq. (2b), we obtain

$$[m\,(T)]^{-1} = \frac{T_g}{T_C^{\mathrm{DS}}}\frac{1}{\phi\,\log_{10}e}\left(1-\frac{T_C^{\mathrm{DS}}}{T}\right). \tag{10}$$

The gray line in the inset is a fitting of the data to Eq. (10) up to T_A, resulting in a ϕ value of 9 and a T_C^{DS} of 314.7 K. Both values are compatible with those listed in Table II for the three dielectric modes $\mu_{1,L}$, $\mu_{1,H}$, and μ_2. These fitting parameters are used to represent the inverse of Eq. (10) on Fig. 6, also as a gray curve, demonstrating good agreement with the experimental values. Thus, *m(T)* is well portrayed by the DS critical-like description in the *N* mesophase.

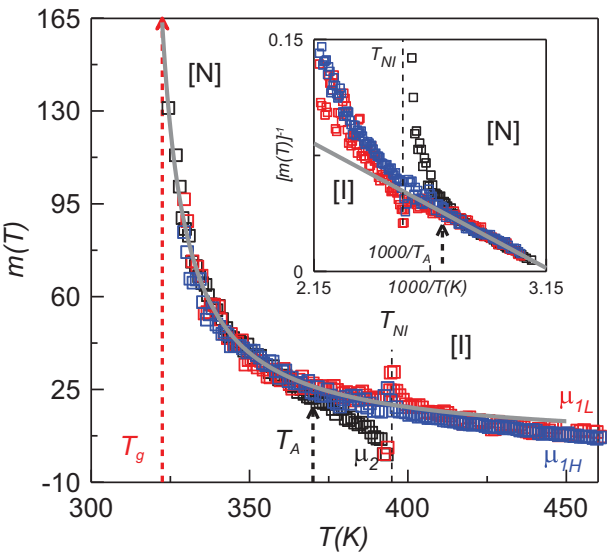

FIG. 6. Results for the temperature-dependent steepness index *m(T)* for the different relaxation modes of *CBO3O.Py* as a function of temperature. The inset shows the linear dependence of the inverse of *m(T)* with the inverse of temperature. The gray line in the inset is a fit of data to Eq. (10) and is drawn in the main figure with $T_C^{\mathrm{DS}} =$ 314.7 K and ϕ exponent of 9.

Recently, Drozd-Rzoska [50] reaffirmed the prevalence of the critical-like description for describing the relaxation time $\tau(T)$ of liquid crystals over the most popular VFT model or other recent proposals [51]. However, based on *m(T)* data, Drozd-Rzoska [50] parametrized the previtreous anomaly for a different set of glass formers as

$$m(T) = \frac{A}{T - T_g^*}, \tag{11}$$

where A is a constant and T_g^* is defined as the virtual glass transition temperature at which $[m(T_g^*)]^{-1} = 0$. In addition, ΔT_g^*, defined as $T_g - T_g^*$, is proposed as the measure of the discontinuity of the glass transition [50]. From Eq. (5) and Eq. (11) it is easy to obtain

$$\frac{d\,\ln\tau(T)}{d(T^{-1})}\frac{\log_{10}e}{T_g} = \frac{A}{T - T_g^*}. \tag{12}$$

From the subsequent integration of Eq. (12), Drozd-Rzoska proposed an activation-critical (AC) formula for the relaxation time [50]:

$$\tau(T) = C_\Omega\left(\frac{T - T_g^*}{T}\right)^{-\Omega}\exp\left(\Omega\left(\frac{T - T_g^*}{T}\right)\right), \tag{13}$$

where C_Ω is a constant and Ω is a power exponent, which can be shown to be related to parameters A, T_g, and T_g^* as follows:

$$\Omega = \frac{AT_g}{T_g^{*2}\,\log_{10}e}. \tag{14}$$

As cited by Drozd-Roska *et al.* [51], Eq. (13) offers a link between the critical-like description and super-Arrhenius (SA) activation features.

Figure 7 illustrates the scenario explored by Eq. (11) on the *CBO3O.Py* crystal dimer. The highest temperature at which Eq. (11) is considered to be valid is denoted by T_r. From a linear fitting of the data from the lowest temperature up to T_r, we obtain T_g^* of the dimer as 312 ± 1 K. This value is taken as common for all the dielectric modes. The inset of Fig. 7 shows an Arrhenius plot of the τ data for the three dielectric modes of *CBO3O.Py*, along with the tentative fittings according to Eq. (13), spanning from T_r to the lowest temperature. Notably, the fittings have been done with the same T_g^*, with only $\ln C_\Omega$ and the Ω power exponent being adjusted. This approach causes a certain discrepancy in T_g for the different modes, ranging from 322.2 K for the μ_2 mode, 322.9 K for the $\mu_{1,H}$ mode, and 324.1 K for the $\mu_{1,L}$ mode. However, the Ω power

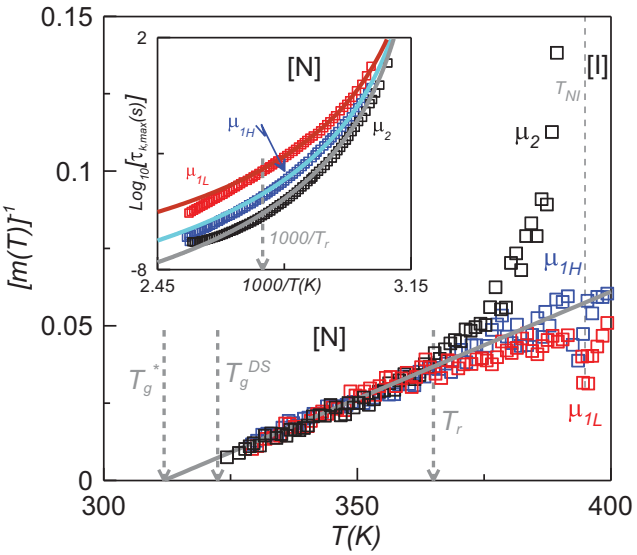

FIG. 7. Results for the inverse of steepness index $[m(T)]^{-1}$ for the different relaxation modes of *CBO3O.Py* are presented as a function of the temperature. The gray line represents a fit of data to Eq. (11) from low temperature up to T_r of about 365 K. The inset shows the relaxation-time data of the different modes as an Arrhenius plot, with the drawn lines representing fittings to Eq. (13).

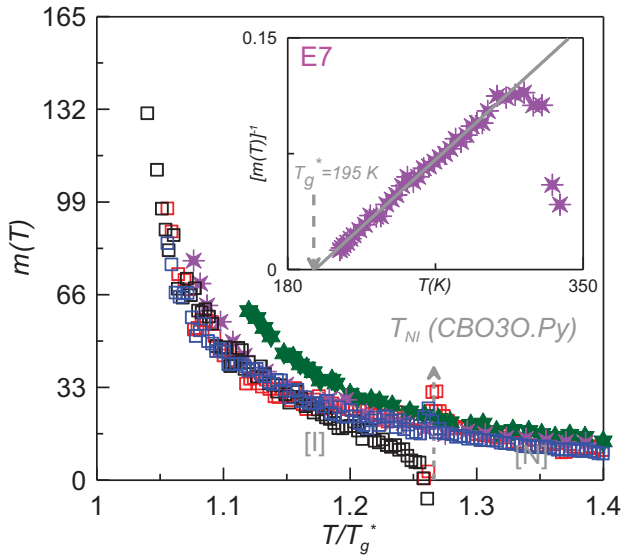

FIG. 8. Results for steepness index $m(T)$ for the different relaxation modes of *CBO3O.Py* (μ_{1L}: □; μ_{1H}: □; μ_2: □) along with the relaxation mode associated with the rotational fluctuations around the short axis of the molecules (δ mode) of *E7* (✶) and *5CB* (★) rodlike liquid crystals as a function of the reduced temperature (T/T_g^*). The inset shows the inverse of steepness index $[m(T)]^{-1}$ for the δ mode of *E7* as a function of the temperature. The gray line is a fit of data to Eq. (11) from low temperature up to T_r of about 300 K.

exponent yields the same value regardless of the dielectric mode, being 12 ± 1. It is likely that this discrepancy of about 2 K in T_g could be minimized if the fittings to Eq. (13) were done simultaneously over three parameters, namely T_g^*, $\ln C_\Omega$, and Ω.

The AC relationship given by Eq. (13) offers a robust tool to portray the relaxation time data for a wide variety of glass formers. Dordz-Rzoska *et al.* [51] considered this formulation to be as powerful as the Mauro Yue Ellison Gupta Allan (MYEGA) equation [52]. A critical-like description based on the DS model for temperatures in the domain of glass transition can be considered as a terminal approximation of the more general AC formula embodied by Eq. (13) [50].

Another intriguing topic to be investigated is the possibility of finding a universal plot of $m(T)$ for several glass liquid crystal formers. As explored in Ref. [10], the attempt to create such a universal plot was made by plotting $m(T)$ against (T/T_{NI}) for two liquid crystal dimers, *CBO7O.Py* and *CB7CB*. While the result was not perfect, it was promising since the T_g/T_{NI} ratio is approximately 0.7 for both compounds. However, it is important to note that the success of such universal plot depends on the similarity of the T_g/T_{NI} ratio among the compounds to be compared. If this ratio varies significantly, the representation fails as a universal plot. Additionally, in a potential universal plot of $m(T)$, the temperature range to be considered should be close to the glass transition temperature. One possible alternative could be plotting $m(T)$ against (T/T_g). However, Eq. (11) offers an interesting possibility if is rewritten as

$$m(T) = \frac{A}{T_g^*} \frac{1}{\frac{T}{T_g^*} - 1}. \tag{15}$$

Figure 8 shows the plot of $m(T)$ against (T/T_g^*) for the *CBO3O.Py* liquid crystal dimer along with two rodlike liquid crystals, *5CB* (pentylcyanobiphenyl) and *E7* (a eutectic mixture of several rodlike liquid crystals). The $m(T)$ data for *5CB* and *E7* were obtained by applying Eq. (5) to the digitalized data of Fig. 2 of Ref. [38] and Fig. 2 of Ref. [34], respectively. The choice of both rodlike liquid crystal compounds, *5CB* and *E7*, for this analysis is based on several considerations. First, both *5CB* and *E7* exhibit a nematic glass transition, and the dynamic data close to the glass transition are available in the literature. Second, the dynamic data for these compounds, particularly in the vicinity of the glass transition, are well described by the DS model as symmetry-selected glass formers, with a ϕ exponent close to 9, as evident in Table III. Third, the inclusion of liquid crystal molecules with different molecular structures is essential for a potential universal plot of $m(T)$.

TABLE III. Dynamic scaling (DS) model parameters for several liquid crystals.

Compound	Mode	T_C^X (K)	ϕ	T_g (K)	Reference
CBO7O.Py	$\mu_{1,L}$	308.1	7.7	317.0	[10]
	$\mu_{1,H}$	304.1	7.6	310.7	
	μ_2	308.6	6.2	310.5	
CB7CB	μ_1	273.1	6.2	275.8	[1]
	μ_2	273.5	7.4	276.2	
E7	δ [a]	200 ± 3	8.7 ± 0.3	208 ± 3	[34]
5CB	δ [a]	197 ± 1	8.8 ± 0.3	207	[38]

[a]This mode in rodlike liquid crystals is identified with the rotational fluctuations around the short axis of the molecule.

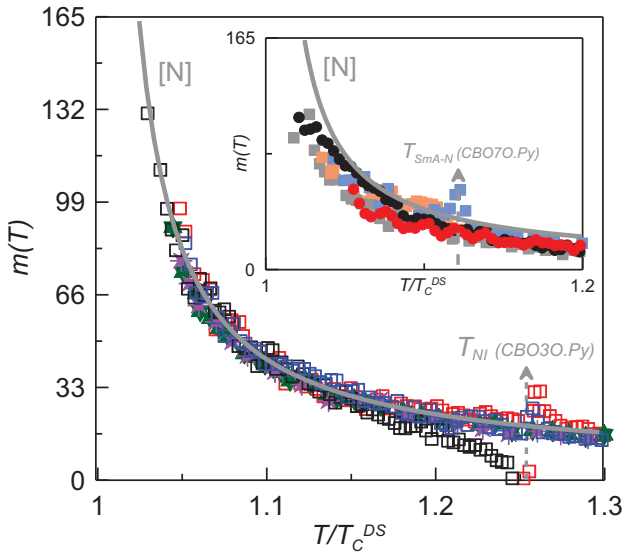

FIG. 9. Results for steepness index $m(T)$ for the different relaxation modes of *CBO3O.Py* (μ_{1L}: □; μ_{1H}: □; μ_2: □) liquid crystals dimer along with the δ mode of *E7* (✶) and *5CB* (★) rodlike liquid crystals are plotted as a function of reduced temperature (T/T_C^{DS}). The gray curve represents Eq. (16) with a ϕ value of 9. The inset shows the same plot as in the main figure but only with *CBO7O.Py* (μ_{1L}:■; μ_{1H}: ■; μ_2: ■) and CB7CB (μ_1:●; μ_2:●) liquid crystal dimers.

This choice allows for a broader exploration of the applicability and generalization of the $m(T)$ behavior across diverse liquid crystal systems. Table III lists relevant DS model data, already published, corresponding to two nematic liquid crystal dimers, *CBO7O.Py* and *CB7CB,* and the two nematic rodlike liquid crystals, *5CB* and *E7*.

The inset of Fig. 8 represents $[m(T)]^{-1}$ as a function of temperature for *E7* data [34]. This plot facilitates the determination of T_g^* of *E7* by fitting the data according to Eq. (11). For 5CB, a T_g^* of 185.7 K is reported in Ref. [50].

It is evident from Fig. 8 that (T/T_g^*) is not the most suitable choice for a universal plot of $m(T)$, as the *5CB* liquid crystal does not exhibit the same trend as the dimer when approaching the glass transition. The value of A/T_g^* for *5CB* can be estimated from Eq. (14) to be about 7, which is substantially different from that of *CBO3O.Py*, which is around 5. The m fragility $[m(T_g)]$ calculated from Eq. (15) yields a value of 157, which is close to the value of 165 that can be extracted from Fig. 6. Drozd-Rzoska [50] considers another rodlike liquid crystal in her study, the *8*OCB*, and the calculated A/T_g^* is also about 7. However, for the *E7,* based on the linear fitting to the data from the inset of Fig. 8, the estimated A/T_g^* is close to 5. Notably, it seems there is no universal value of A/T_g^* for rodlike liquid crystals.

Recalling the simplest DS model, Eq. (10), considering that $T_C^{DS}/T_g \approx 1$, it can be reformulated as

$$m(T) \approx \phi \log_{10} e \frac{\left(\frac{T}{T_C^{DS}}\right)}{\left(\frac{T}{T_C^{DS}}\right)^{-1}}, \qquad (16)$$

and thus, Eq. (16) enlightens the way for a universal plot of $m(T)$ as a function of (T/T_C^{DS}). Figure 9 shows how the data for both monomers and dimer collapse into a common trend. The gray curve, corresponding to a ϕ value of 9, portrays the plotted data exceptionally well. This suggests that the curve is valid not only for *CBO3O.Py* but also for other compounds that follow the DS model and are categorized as symmetry-selected glass formers. It is a noteworthy observation that these compounds follow the same trend of $m(T)$ with (T/T_C^{DS}), yet they differ in their m fragility at the glass transition. Indeed, the observation that less fragile compounds reach the glass transition at higher (T/T_C^{DS}) implies their inability to accommodate molecular cooperative motions at lower temperatures.

The $m(T)$ asymptotic trend of Fig. 9 suggests significant dynamic changes that all these compounds, regardless of their internal structure, must undergo equally. However, not all of them can achieve these changes as temperature decreases. Probably, liquid crystal dimers are structurally better designed than liquid crystal monomers to accommodate the highly cooperative motions at lower temperatures, before the dynamic breakdown that implies the glass transition.

The inset of Fig. 9 displays the curve given by Eq. (16), considered as representative of the behavior of liquid crystal categorized as symmetry-selected glass formers and data from two additional dimers, *CBO7O.Py* and *CB7CB*, sourced from other published studies [1,10]. Unfortunately, the scatter of data from the common trend (represented by the gray line in the inset of Fig. 9) is evident due to the inclusion of data as a consequence of the ϕ exponent significantly different from 9.

The discrepancy in the ϕ exponent for both *CBO7O.Py* and *CB7CB* liquid crystal dimers in relation to the *CBO3O.Py* and the other liquid crystals listed in Table III prompts the question of their uniaxial symmetry. Despite possessing uniaxial symmetry akin to liquid crystal monomers and *CBO3O.Py* liquid crystal dimer, the molecular flexibility in *CBO7O.Py* and *CB7CB* may contribute to a reduction in the dominating symmetry. This effect is not observed in *CBO3O.Py* liquid crystal, likely due to the short length of the spacer, which causes a more rigid molecular structure similar to that of the liquid crystal monomers.

IV. CONCLUDING REMARKS

The *CBO3O.Py* liquid crystal dimer is the shorter chain length compound within the highly nonsymmetric pyrene-based series of liquid crystal dimers (*CBOnO.Py*, with n ranging from 3 to 11). Similar to other compounds in this series, the nematic mesophase displays three dielectric relaxation modes, namely, $\mu_{1,L}$, $\mu_{1,H}$, and μ_2, with interpretations with those observed in other compounds of the series. However, while *CBO7O.Py* exhibits two glass transitions at different temperatures, one identified with $\mu_{1,L}$ and the other associated with both $\mu_{1,H}$ and μ_2 [10], *CBO3O.Py* only exhibits one glass transition temperature. This has been experimentally proved elsewhere by TSDC [9] and corroborated by the DS model in the present study.

The data analysis of *CBO3O.Py* liquid crystal dimer has been centered to discriminate the most suitable formulation to describe the dielectric relaxation-time data with temperature, from the isotropic state through the nematic mesophase down to the vicinity of the glass transition. Two formulations were

initially tested, namely, the Vogel-Fulcher-Tammann (VFT) and the critical-like description that combines the dynamic scaling model (DSM) for temperatures in the vicinity of the glass transition, and the mode-coupling theory (MCT) for higher temperatures. Again, as in other similar studies for other liquid crystals, the critical-like description seems to be superior to VFT, giving rise to only one glass transition temperature for the different relaxation modes.

From the recent work of Drozd-Rzoska [50], which focused on the evolution of the steepness index *m(T)* with temperature, a more general formulation to describe the dielectric relaxation-time data was considered, namely the activation-critical (AC) model. This model was tested for *CBO3O.Py* liquid crystal dimer. It is noteworthy that the dynamic scaling (DS) model is a terminal approximation for data close to the glass transition. In a first step, the activation-critical formulation was tested as a universal plot for the temperature-dependent steepness index *m(T)*.

The application of the critical-like description to *CBO3O.Py* in the vicinity of glass transition yields a ϕ exponent close to 9, regardless of the dielectric relaxation mode. This value is universal for symmetry-selected glass formers, such as rodlike liquid crystal monomers with uniaxial symmetry. Strangely, other dimers like *CBO7O.Py* and *CB7CB* exhibit ϕ exponents significantly different from 9. It is argued that the shorter length spacer in *CBO3O.Py* makes it more rigid, thereby preserving the uniaxial symmetry of the molecule.

Considering the temperature-dependent steepness index *m(T)*, a universal plot has been possible to be achieved using the equations of the DS model for those compounds with ϕ exponents close to 9, which fall into the category of symmetry-selected glass formers. However, for other dimers described by the DS model with ϕ exponents different from 9, there is a noticeable scatter of data that blurs the obtained universal trend for the compounds categorized as symmetry-selected glass formers and following the DS model.

Finally, upon a more detailed examination of Fig. 9, the symmetry-selected glass formers with greater molecular flexibility can accommodate highly cooperative motions at lower temperatures, consequently increasing the *m* fragility at the glass transition.

The data that support the findings of this study are openly available in Zenodo [53].

ACKNOWLEDGMENTS

N.S. acknowledges financial support of the Slovenian Research Agency (Grant No. P1-0192). M.R.d.l.F. acknowledges the financial support by Eusko Jaurlaritza-Basque Government under Project No. IT1458-22.

[1] D. O. López, N. Sebastián, M. R. de la Fuente, J. C. Martínez-García, J. Salud, M. A. Pérez-Jubindo, S. Diez-Berart, D. A. Dunmur, and G. R. Luckhurst, J. Chem. Phys. **137**, 034502 (2012).

[2] N. Sebastián, M. R. de la Fuente, D. O. López, M. A. Pérez-Jubindo, J. Salud, S. Diez-Berart, and M. B. Ros, J. Phys. Chem. B **115**, 9766 (2011).

[3] N. Sebastián, M. R. de la Fuente, D. O. López, M. A. Pérez-Jubindo, J. Salud, and M. B. Ros, J. Phys. Chem. B **117**, 14486 (2013).

[4] S. Diez-Berart, D. O. López, J. Salud, J. A. Diego, J. Sellares, B. Robles-Hernández, M. R. de la Fuente, and M. B. Ros, Materials **8**, 3334 (2015).

[5] N. Sebastián, D. O. López, B. Robles-Hernández, M. R. de la Fuente, J. Salud, M. A. Pérez-Jubindo, D. A. Dunmur, G. R. Luckhurst, and D. J. B. Jackson, Phys. Chem. Chem. Phys. **16**, 21391 (2014).

[6] B. Robles-Hernández, N. Sebastián, M. R. de la Fuente, D. O. López, S. Diez-Berart, J. Salud, M. B. Ros, D. A. Dunmur, G. R. Luckhurst, and B. A. Timini, Phys. Rev. E **92**, 062505 (2015).

[7] D. O. López, B. Robles-Hernández, J. Salud, M. R. de la Fuente, N. Sebastián, S. Diez-Berart, X. Jaen, D. A. Dunmur, and G. R. Luckhurst, Phys. Chem. Chem. Phys. **18**, 4394 (2016).

[8] B. Robles-Hernández, N. Sebastián, J. Salud, S. Diez-Berart, D. A. Dunmur, G. R. Luckhurst, D. O. López, and M. R. de la Fuente, Phys. Rev. E **93**, 062705 (2016).

[9] J. A. Diego, J. Sellares, S. Diez-Berart, J. Salud, J. C. Cañadas, M. Mudarra, D. O. López, M. R. de la Fuente, and M. B. Ros, Liq. Cryst. **44**, 1007 (2017).

[10] D. O. López, J. Salud, M. R. de la Fuente, N. Sebastián, and S. Diez-Berart, Phys. Rev. E **97**, 012704 (2018).

[11] C. T. Imrie and G. R. Luckhurst, in *Handbook of Liquid Crystals*, edited by D. Demus, J. W. Goodby, G. W. Gray, H. W. Speiss, and V. Vill (Wiley VCH, Weinheim, 1998), Vol. 2B, Chap. X, p. 801.

[12] M. Cestari, S. Diez-Berart, D. A. Dunmur, A. Ferrarini, M. R. de la Fuente, D. J. B. Jackson, D. O. López, G. R. Luckhurst, M. A. Pérez-Jubindo, R. M. Richardson, J. Salud, B. A. Timimi, and H. Zimmermann, Phys. Rev. E **84**, 031704 (2011).

[13] H. J. Coles and M. N. Pivnenko, Nature (London) **436**, 997 (2005).

[14] G. S. Attard, C. T. Imrie, and F. E. Karasz, Chem. Mater. **4**, 1246 (1992).

[15] N. Sebastián, B. Zupančic, B. Zalar, D. O. López, J. Salud, V. López de Rioja, R. Levit, B. Robles-Hernández, M. R. de la Fuente, N. Gimeno, M. B. Ros, and S. Diez-Berart, Phys. Chem. Chem. Phys. **25**, 2486 (2023).

[16] M. Stocchero, A. Ferrarini, G. J. Moro, D. A. Dunmur, and G. R. Luckhurst, J. Chem. Phys. **121**, 8079 (2004).

[17] W. Maier and G. Z. Meier, Naturforsch. A **16**, 262 (1961).

[18] P. L.Nordio, and G. Rigatti, and U. Segre, Mol. Phys. **25**, 129 (1973).

[19] H. R. Zeller, Phys. Rev. Lett. **48**, 334 (1982).

[20] A. Drozd-Rzoska, S. J. Rzoska, and M. Janik, in *Glassy Dynamics of Rod-Like Liquid Crystals: The Influence of Molecular Structure*, NATO Sci. Series II, Soft Matter Under Exogenic Impacts, Vol. 242, edited by S. J. Rzoska and V. Mazur (Springer-Verlag, Berlin, 2007).

[21] A. R. Brás, M. Dionísio, H. Huth, C. Schick, and A. Schönhals, Phys Rev. E **75**, 061708 (2007).
[22] M. H. Cohen and G. S. Grest, Phys Rev. B **20**, 1077 (1979).
[23] G. Adam and J. H. Gibbs, J. Chem. Phys. **43**, 139 (1965).
[24] T. Hecksher, A. B. Nielsen, N. B. Olsen, and J. C. Dyre, Nat. Phys. **4**, 737 (2008).
[25] G. B. McKenna, Nat. Phys. **4**, 673 (2008).
[26] J. P. Eckmann and I. Procaccia, Phys. Rev. E **78**, 011503 (2008).
[27] F. Mallamace, C. Branca, C. Corsaro, N. Leone, J. Spooren, S. H. Chen, and E. Stanley, Proc. Natl Acad. Sci. **107**, 22457 (2010).
[28] J. Souletie, J. Phys. France **51**, 883 (1990).
[29] R. H. Colby, Phys. Rev. E **61**, 1783 (2000).
[30] B. M. Erwin and R. H. Colby, J. Non-Cryst. Solids **307**, 225 (2002).
[31] P. C. Hohenberg and B. I. Halperin, Rev. Mod. Phys. **49**, 435 (1977).
[32] J. V. Sengers, D. Bedeaux, P. Mazur, and S. C. Greer, Physica A **104**, 573 (1980).
[33] J. C. Martínez-García, S. J. Rzoska, A. Drozd-Rzoska, and J. Martínez-García, Nat. Commun. **4**, 1823 (2013).
[34] A. Drozd-Rzoska, S. J. Rzoska, and M. Paluch, J. Chem. Phys. **129**, 184509 (2008).
[35] W. Götze and L. Sjögren, Rep. Prog. Phys. **55**, 241 (1992).
[36] A. Schönhals, F. Kremer, A. Hofmann, E. W. Fischer, and E. Schlosser, Phys Rev. Lett. **70**, 3459 (1993).
[37] F. Kremer and A. Schönhals, *Broadband Dielectric Spectroscopy* (Springer, Berlin, 2003).
[38] A. Drozd-Rzoska, J. Chem. Phys. **130**, 234910 (2009).
[39] C. A. Angell, in *Relaxations in Complex Systems*, edited by K. Ngai, and G. B. Wright (Springfield, Washington DC, 1985).
[40] C. A. Angell, J. Phys. Chem. Solids **49**, 863 (1988).
[41] C. A. Angell, J. Non-Cryst. Solids **131–133**, 13 (1991).
[42] R. Puertas, M. A. Rute, J. Salud, D. O. López, S. Diez, J. K. van Miltenburg, L. C. Pardo, J. Ll. Tamarit, M. Barrio, M. A. Pérez-Jubindo, and M. R. de la Fuente, Phys. Rev. B **69**, 224202 (2004).
[43] R. Puertas, J. Salud, D. O. López, M. A. Rute, S. Diez, J. Ll. Tamarit, M. Barrio, M. A. Pérez-Jubindo, M. R. de la Fuente, and L. C. Pardo, Chem. Phys. Lett. **401**, 368 (2005).
[44] D. J. Plazek and K. L. Ngai, Macromolecules **24**, 1222 (1991).
[45] R. Bohmer and C. A. Angell, Phys. Rev. B **45**, 10091 (1992).
[46] A. Drozd-Rzoska and S. J. Rzoska, Phys. Rev. E **73**, 041502 (2006).
[47] P. Cusmin, M. R. de la Fuente, J. Salud, M. A. Pérez-Jubindo, S. Diez-Berart, and D. O. López, J. Phys. Chem. B **111**, 8974 (2007).
[48] F. Stickel, E. W. Fischer, and R. Richert, J. Chem. Phys. **102**, 6251 (1995).
[49] R. Richert, F. Stickel, R. S. Fee, and M. Maroncelli, Chem. Phys. Lett. **229**, 302 (1994).
[50] A. Drozd-Rzoska, Sci. Rep. **9**, 6816 (2019).
[51] A. Drozd-Rzoska, S. J. Rzoska, and S. Starzonek, Prog. Mater. Sci. **134**, 101074 (2023).
[52] J. C. Mauro, Y. Yue, A. J. Ellison, P. K. Gupta, and D. C. Allan, Proc. Natl. Acad. Sci. USA **106**, 19780 (2009).
[53] Zenodo, doi:10.5281/zenodo.12683168.